

What Makes the Family of Barred Disc Galaxies So Rich: Damping Stellar Bars in Spinning Haloes

Angela Collier^{1*}, Isaac Shlosman^{1,2†}, Clayton Heller³

¹ *Department of Physics & Astronomy, University of Kentucky, Lexington, KY 40506-0055, USA*

² *Theoretical Astrophysics, Graduate School of Science, Osaka University, Osaka 560-0043, Japan*

³ *Department of Physics, Georgia Southern University, Statesboro, GA 30460, USA*

Accepted ?; Received ??; in original form September 29, 2017

ABSTRACT

We model and analyze the secular evolution of stellar bars in spinning dark matter (DM) haloes with the cosmological spin $\lambda \sim 0 - 0.09$. Using high-resolution stellar and DM numerical simulations, we focus on angular momentum exchange between stellar discs and DM haloes of various axisymmetric shapes — spherical, oblate and prolate. We find that stellar bars experience a diverse evolution which is guided by the ability of parent haloes to absorb angular momentum, J , lost by the disc through the action of gravitational torques, resonant and non-resonant. We confirm that dynamical bar instability is accelerated via resonant J -transfer to the halo. Our main findings relate to the long-term, secular evolution of disc-halo systems: with an increasing λ , bars experience less growth and basically dissolve after they pass through vertical buckling instability. Specifically, with increasing λ , (1) The vertical buckling instability in stellar bars collides with inability of the inner halo to absorb J — this emerges as the main factor weakening or destroying bars in spinning haloes; (2) Bars lose progressively less J , and their pattern speeds level off; (3) Bars are smaller, and for $\lambda \gtrsim 0.06$ cease their growth completely following buckling; (4) Bars in $\lambda > 0.03$ halos have ratio of corotation-to-bar radii, $R_{\text{CR}}/R_b > 2$, and represent so-called slow bars without offset dust lanes. We provide a quantitative analysis of J -transfer in disc-halo systems, and explain the reasons for absence of growth in fast spinning haloes and its observational corollaries. We conclude that stellar bar evolution is substantially more complex than anticipated, and bars are not as resilient as has been considered so far.

Key words: methods: dark matter — galaxies: evolution — galaxies: formation — galaxies: interactions — galaxies: kinematics and dynamics

1 INTRODUCTION

Galactic discs are embedded in dark matter (DM) haloes of a range in the cosmological spin parameter $\lambda \equiv J_h/\sqrt{2}M_{\text{vir}}R_{\text{vir}}v_c$, where J_h is the DM angular momentum, M_{vir} and R_{vir} — the halo virial mass and radius, and v_c — circular velocity at R_{vir} , with the mean value $\lambda = 0.035 - 0.04 \pm 0.005$ (e.g., Bullock et al. 2001; Hetzner & Burkert 2006; Knebe & Power 2010). While discs are supported by rotation, haloes are dominated by the random motions. When discs are embedded in DM haloes, they can serve as sources of the angular momentum, J , and haloes are perceived as sinks of J (e.g., Sellwood 1980; Debattista & Sellwood 2000; Athanassoula

2003; Martinez-Valpuesta et al. 2006). Hence, the angular momentum generally is expected to flow from the disc to the parent halo, especially when galactic bars form and facilitate the J -transfer.

This description is oversimplified, because it is based on numerical simulations of nonrotating, isolated DM haloes. Halos produced in cosmological simulations with a range of λ usually lack resolution and were not analyzed similarly. Recently, Saha & Naab (2013) have shown that the bar instability rise time is shortened with increasing λ , but their analysis has been limited to the instability itself. Furthermore, Long et al. (2014) demonstrated that the J -transfer from the disc to its parent halo over *secular* time depends on λ , and its efficiency decreases sharply with increasing λ — an effect which directly opposes that of Saha & Naab. While Long et al. have determined this for spherical haloes only, the importance of this effect requires a broader approach.

* E-mail: angela.collier@uky.edu

† E-mail: shlosman@pa.uky.edu

Disc-halo interaction in *spinning* haloes has been also analysed by Petersen et al. (2016), which concluded that the DM halo spin does not affect the stellar bar evolution. However, they have limited the range of λ to less than 0.03 and their analysis included only the first 4 Gyr of the bar evolution. In other words, again it was limited to the time period of the bar instability itself, prior to the vertical buckling of stellar bars, completely avoiding their secular evolution.

In this paper, we demonstrate that the dependence of J -transfer on the cosmological spin of parent DM haloes over secular time is strong and a universal one, independent of the halo shape — oblate, prolate or spherical. We demonstrate that stellar bar evolution is profoundly affected by the disc-halo angular momentum transfer over wide range of λ and time. Furthermore, we analyze the corollaries of J -transfer on the evolution of galactic stellar bars.

Angular momentum redistribution in astrophysical systems is one of the main drivers of their evolution. Gravitational torques play a major role in this process on all spatial scales, and in a broad range of systems, from the Earth-Moon, to planetary systems, close stellar binaries, formation of compact objects, galaxy interactions, etc. At some instances they act on dynamical time scales, i.e., time scale comparable with the crossing time of a system. In other cases, they act on time scales much longer than dynamical ones — so-called secular time scales, e.g., in accretion discs in stellar systems and compact objects.

Any departure from axial symmetry triggers and amplifies gravitational torques. In the context of stellar discs immersed in DM haloes, both can exhibit departures from axial symmetry. These asymmetries can be related to the formation process of such systems, develop spontaneously, or as a result of interactions.

For example, DM haloes appear universally triaxial when forming (e.g., Allgood et al. 2006; Hetzner & Burkert 2006), but tend to be axisymmetric in the contemporary universe (e.g., Rix & Zaritsky 1995; Merrifield 2002). This process has been demonstrated in numerical simulations with baryons which modify the halo shapes (Berentzen & Shlosman 2006).

Stellar discs can break their axial symmetry spontaneously (e.g., Hohl 1971; Athanassoula 1992a; Sellwood & Wilkinson 1993; Knapen et al. 1995a,b), or as a result of external triggering (e.g., Holmberg 1941; Toomre & Toomre 1972; Noguchi 1987; Gerin et al. 1990). If two gravitational quadrupoles are present in the system, e.g., triaxial DM halo and a stellar bar, the gravitational torques act to synchronise their rotation, by exchange of the angular momentum, although the efficiency of this process depends on a number of parameters.

The flow of the angular momentum in the disc-halo system has been a target of investigation for a long time. Theoretically, it has been understood to involve resonant and non-resonant components (e.g., Lynden-Bell & Kalnajs 1972; Tremaine & Weinberg 1984; Weinberg 1985). Numerically, it has been detected in the first simulations involving a live DM halo (Sellwood 1980), and analysed thereafter (e.g., Debattista & Sellwood 2000; Athanassoula 2003; Martinez-Valpuesta et al. 2006; Weinberg & Katz 2007a,b; Dubinski et al. 2009; Villa-Vargas et al. 2009). These works have focused on J -transfer between barred discs and *non-rotating* DM haloes. In such systems, the halo absorbs

the angular momentum, and this process involves resonant and non-resonant interactions between DM and stellar orbits (Athanassoula 2003; Martinez-Valpuesta et al. 2006; Weinberg & Katz 2007a,b). However, the exact fraction of resonant transfer has been never measured, although Dubinski et al. (2009) counted about 20–30% of the halo particles appear to be trapped in major resonances at some time of their history.

Action of gravitational torques can be described within the context of a non-local viscosity (e.g., Larson 1984; Lin & Pringle 1987; Shlosman 1991), causing redistribution of mass and angular momentum in the system. Disc stars and gas can lose or acquire angular momentum. Stars and gas that are located inside the corotation radius, lose J and move in gradually. When the gaseous component is present, the rate of loss of J is amplified due to shocks — unlike stars, the gas cannot reside on intersecting orbits. Bar formation leads to an increased central concentration in both components that lose J , i.e., not only in gas but also in stars (Dubinski et al. 2009). The outer regions of discs, outside the corotation radii, can absorb some J and expand, but little mass resides there and so its capacity to absorb J is low. In contrast, the non-rotating haloes have a large capacity to absorb J .

The evolutionary corollaries for a disc-halo system redistributing angular momentum appear to be more obvious for the disc, which loses a non-negligible amount of J and develops a bar. Beyond this fact not much is known — isolated haloes have been studied mostly non-rotating, while cosmological haloes lack numerical resolution so essential for capturing the resonant interactions, as we have noted above.

The most general questions that can be asked about implications for observations of galactic bars and disc galaxy evolution can be summed as follows. Does the lifetime of the bar depend on the spin of its parent DM halo? Does the bar strength and its pattern speed? Are the bar size and other properties affected? Are there any observable effects on the shape, size, concentration, etc. of galactic discs and their bulges? And finally, is there a measurable effect on the halo properties, at least for the inner haloes?

This paper is structured as following. Numerical aspects and initial conditions are described in §2, and our results of numerical modeling are presented in §3. Next, we discuss the observational corollaries of our results and perform additional tests. Conclusions are given in the last section.

2 NUMERICAL TECHNIQUES

We use the N -body part of the tree-particle-mesh Smoothed Particle Hydrodynamics (SPH/ N -body) code GIZMO originally described in Hopkins (2015). The units of mass and distance are taken as $10^{10} M_{\odot}$ and 1 kpc, respectively. The resulting time unit is 1 Gyr. We use $N_h = 7.2 \times 10^6$ particles for the DM halo, and $N_d = 8 \times 10^5$ for stars, in order to have mass ratio of DM particles to stellar particles of unity. Gas component is neglected in this work. For the convergence test, we have doubled the number of particles to $N_h = 1.44 \times 10^7$ and $N_d = 1.6 \times 10^6$ in some models. The high-resolution models resulted in a qualitatively and quantitatively similar evolution to the lower resolution models. The number of particles in the range of $\sim 10^6 - 10^7$

was found to be sufficient to account for resonant interactions of stellar bar and halo orbits in disc-halo systems (Dubinski et al. 2009).

The gravitational softening used in the current modeling is $\epsilon_{\text{grav}} = 25 \text{ pc}$ for stars and DM. The opening angle θ of the tree code has been reduced from 0.5–0.7 used in cosmological simulations to 0.4, which increases the quality of force calculations. Our models have been run at least for 10 Gyr with an energy conservation of 0.05% and angular momentum conservation of 0.03% over this time.

2.1 Initial Conditions

For the initial conditions we used the method introduced by Rodionov & Sotnikova (2006), see also Rodionov et al. (2009) and Long et al. (2014), with some modifications. The basic idea of this iterative approach follows the principle that non-equilibrium systems will evolve in the direction of an equilibrium. We start by generating a particle distribution with a chosen density distribution.

We use the standard definition of oblate and prolate ellipsoids, namely, it is oblate when $a = b > c$, and prolate when $c > a = b$. The c axis always points along the z direction, and c and a are the polar and equatorial DM halo axes. Note that this definition includes only the axisymmetric objects, and differs from definition used by Allgood et al. (2006), who invoked triaxial ellipsoids with $a > b > c$.

In order to obtain prolate and oblate configurations from the spherical one, we have multiplied the z coordinates of particles by a factor $q = c/a$ and divided the x and y coordinates by $q^{1/2}$. This method preserves the density distribution. To maintain consistency between the models, the product of principal axes, abc , representing the halo volume, was kept fixed.

An iteration starts by evolving the particles from their initial positions and zero velocities for a period of 0.3 Gyr. Then for each of the particles in the initial unevaluated distribution, we locate the nearest evolved particle and copy its velocity. The directions of these updated velocities are then randomized to maintain the isotropic velocity dispersion. This is the end of an iteration.

Typically, about 50 iteration are required to reach an equilibrium which has the original density distribution and self-consistent velocities.

To test the equilibrium, isolated haloes were evolved for 3 Gyr, checking the invariance of the virial ratio of the system and its velocity dispersions.

For models with discs embedded in DM haloes, we have iterated as above in the frozen disc potential. As the iterations do not change the halo mass profile, we have calculated the disc rotational and dispersion velocities only once, testing if the disc remains in equilibrium after the halo iterations.

The disc has been constructed as a pure exponential, ignoring the bulge, and its volume density is given by

$$\rho_d(R, z) = \left(\frac{M_d}{4\pi h^2 z_0} \right) \exp(-R/h) \text{sech}^2\left(\frac{z}{z_0}\right), \quad (1)$$

where $M_d = 6.3 \times 10^{10} M_\odot$ is the disk mass, $h = 2.85 \text{ kpc}$ is its radial scalelength, and $z_0 = 0.6 \text{ kpc}$ is the scaleheight. R and z represent the cylindrical coordinates.

The halo density is given by Navarro et al. (1996, hereafter NFW),

$$\rho_h(r) = \frac{\rho_s e^{-(r/r_t)^2}}{[(r+r_c)/r_s](1+r/r_s)^2} \quad (2)$$

where $\rho(r)$ is the DM density in spherical coordinates, ρ_s is the (fitting) density parameter, and $r_s = 9 \text{ kpc}$ is the characteristic radius, where the power law slope is (approximately) equal to -2 , and r_c is a central density core. We used the Gaussian cutoffs at $r_t = 86 \text{ kpc}$ for the halo and $R_t = 6h \sim 17 \text{ kpc}$ for the disc models, respectively. The halo mass is $M_h = 6.3 \times 10^{11} M_\odot$, and halo-to-disc mass ratio within R_t is 2.

Three halo shapes have been implemented. Spherical haloes with polar-to-equatorial axis ratios, $q = c/a = 1$, oblate haloes with $q = 0.8$, and prolate haloes with $q = 1.2$.

All DM halo models have a small flat density core of $r_c = 1.4 \text{ kpc}$ for numerical reasons.

To spin up the DM haloes, we have reversed the tangential velocities of a fraction of retrograde (with respect to the disc rotation) DM particles. The fraction of reversed particles is adjusted in order to give the halo prescribed λ value, in the range of $0 - 0.09$. The implemented velocity reversals preserve the solution to the Boltzmann equation and do not alter the DM density profile or velocity magnitudes (Lynden-Bell 1960; Weinberg 1985; Long et al. 2014). For axisymmetric haloes, the invariance under velocity reversals is a direct corollary of the Jeans (1919) theorem (see also Binney & Tremaine 2008).

Disc radial and vertical dispersion velocities have been taken as

$$\sigma_R(R) = \sigma_{R,0}(R) \exp(-R/2h) \quad (3)$$

$$\sigma_z(R) = \sigma_{z,0}(R) \exp(-R/2h) \quad (4)$$

where $\sigma_{R,0} = 120 \text{ km s}^{-1}$ and $\sigma_{z,0} = 100 \text{ km s}^{-1}$. This leads to the global minimum in the Toomre's parameter $Q \sim 1.6$ at $R \sim 2.4h$ (Toomre 1964). Q increases toward the centre and the outer disc.

Note, that for the purpose of clearly resolving the inner regions of stellar discs, we have constructed the initial conditions such that long bars develop. In addition, in order to comfortably resolve the initial phase of the bar instability, we have decided on slightly 'hotter' discs (e.g., Athanassoula & Sellwood 1986). The result of this choice is that the buckling instability happens slightly later in time. These decisions, while being beneficial for the follow up analysis, do not affect the physics discussed here.

Hence the only difference between our disc-halo models are shapes of DM haloes and their spin λ . The models have been denoted in the following way. All models are prograde with their name starting with P . This letter is followed by the value of λ multiplied by 1000, and followed by the value of q multiplied by 10. Note, we use a capital Q in the model name, not to be confused with the Toomre's parameter. For example, P45Q12 means a prograde model with $\lambda = 0.045$, and $q = 1.2$. We define the Standard Model as that of a non-rotating spherical DM halo, P00Q10. Model P90Q12 was not run due to the difficulty with initial conditions.

3 RESULTS

For each q , all the models have identical mass distribution. Moreover, for different q values, the mass distributions are the same. All models have been evolved for 10 Gyr. This time scale corresponds roughly to observationally inferred, maximally uninterrupted evolution of galactic discs by major mergers (e.g., Gilmore et al. 2002). Discs start axisymmetric, and develop stellar bars which evolve with time. To quantify this evolution, we follow the bar amplitudes, A_2 , their pattern speeds, Ω_b , and their major axes, R_b . The bar strength has been defined as the amplitude of the Fourier $m = 2$ mode,

$$\frac{A_2}{A_0} = \frac{1}{A_0} \sum_{i=1}^{N_d} m_i e^{2i\phi_i}, \quad (5)$$

where we sum over stellar particles with $R \leq 14$ kpc, and mass $m = m_i$ at azimuthal angles ϕ_i . The amplitude of the $m = 2$ mode has been normalized by the monopole term A_0 . Ω_b is obtained from the phase angle $\phi = 0.5 \tan^{-1}[\text{Im}(A_2)/\text{Re}(A_2)]$ evolution with time.

We divide the evolution into two phases. The dynamical phase consists of the bar instability and terminates with the *first* vertical buckling instability of the bar and formation of boxy/peanut-shaped bulge (e.g., Combes et al. 1990; Pfenniger & Friedli 1991; Raha et al. 1991; Patsis et al. 2002; Athanassoula 2005; Martinez-Valpuesta et al. 2006; Berentzen et al. 2007). Such bulges differ from the classical bulges which are supported mainly by stellar dispersion velocities, and correspond to the spheroidal component (e.g., review by Kormendy & Kennicutt 2004). The peanut-shaped bulges have different kinematics and origin compared to the classical bulges.

This buckling weakens the bar but does not dissolve it (Martinez-Valpuesta & Shlosman 2004). The weakening of the bar is dynamic and substantial — A_2 decreases sharply during this process. Recurrent bucklings act to increase the size of the bulge (Martinez-Valpuesta & Shlosman 2005; Martinez-Valpuesta et al. 2006), and have other effects on the bar evolution. Single and double bucklings have been observed in the models presented here (see section 3.2 and Figure 3). Following the first buckling, the bar enters its next phase, that of a secular evolution.

3.1 Evolution of bar amplitude in spinning haloes

Figure 1 displays the bar evolution for all models with various halo shapes and along the λ sequence, while Figure 2 focuses on a direct comparison between different halo shapes with identical λ . Clearly, substantial differences between models exist along both sequences.

First, the bar instability time scale shortens with increasing λ for each of the halo shapes (Figs. 1 and 2), as first noted by Saha & Naab (2013) and Long et al. (2014) for spherical haloes. The most dramatic change appears for the oblate and prolate haloes, where the bar reaches its peak at $t \sim 2.2$ Gyr for $\lambda = 0.09$, i.e., P90, compared to ~ 6 Gyr for $\lambda = 0$, P00 models. This constitutes a delay of ~ 4 Gyr compared to the ~ 2 Gyr for spherical models. Hence the halo shape affects the bar instability profoundly.

Second, and probably of more interest, the *secular*

growth of the bar after the first vertical buckling weakens with λ , for all halo shapes. Compared to the non-rotating models, those with $\lambda \gtrsim 0.03$ display a slower growth in A_2 and even its leveling off at a later time. Models with $\lambda \gtrsim 0.06$ show basically no growth in A_2 after the first buckling. At the end of the runs, bars in spherical haloes with $\lambda \gtrsim 0.06$ exhibit the lowest amplitudes in A_2 , while oblate models exhibit the highest amplitudes. Overall, oblate, spherical and prolate haloes with larger λ impede the secular growth of the stellar bars. This conclusion confirms and strengthens that of Long et al. (2014).

Third, with the exception of prolate halo models with $\lambda \lesssim 0.03$, the maximal bar amplitude before the first buckling is similar in all models (Fig. 1).

Fourth, at the A_2 peak, just before the first buckling, one can observe a plateau. The duration of this plateau (i.e., its width) varies systematically among the models of each halo shape, and increases with λ .

And fifth, the drop in the amplitude A_2 , i.e., ΔA_2 , immediately following the first buckling anticorrelates with λ for oblate and spherical models. In other words, A_2 after buckling reaches a deeper minimum for larger λ . Essentially, in spinning haloes the bar nearly dissolves after buckling, with $A_2 \lesssim 0.1$. This trend is noisier for the prolate models — still the overall trend is clearly in tandem with other halo shape models (Fig. 1).

3.2 Evolution of bar vertical buckling amplitude in spinning haloes

The first vertical buckling time of stellar bars differs between the models — the bar instability time scale depends on the halo shape and its λ . The disc models are identical in all cases, so there is no dependency on disc properties. We, therefore, take a look at the Fourier amplitude of the vertical buckling in these models, A_{1z} , in the rz -plane which is oriented along the bar major axis (Fig. 3). We normalize this amplitude by A_0 calculated earlier.

Three trends can be observed here. First, the buckling happens earlier for higher λ . Second, it happens earlier in prolate haloes, followed by the spherical and then by the oblate ones. Third, in spherical haloes, the amplitude decreases with increasing λ , for $\lambda \lesssim 0.06$, then shows no preferred trend. It exhibits an opposite behavior in prolate models. No dependence of A_{1z} maximum on λ is seen in oblate haloes. Lastly, $\lambda \lesssim 0.03$ prolate models experience a double buckling, and hence exhibit two maxima in A_{1z} .

3.3 Evolution of bar pattern speed in spinning haloes

Evolution of bar amplitude has a direct corollary on its rate of loss of angular momentum. To display the kinematic properties of stellar bars in spinning haloes, we plot Ω_b evolution in Figure 4. A few trends are observable here. First, the pattern speed of the bar at the end of the simulation strongly correlates with λ . This is a consequence of the secular evolution of the bar, which does not regrow in amplitude after buckling in models with higher λ . Consequently, the bar and hence the disc, lose different amounts of angular momentum in the models.

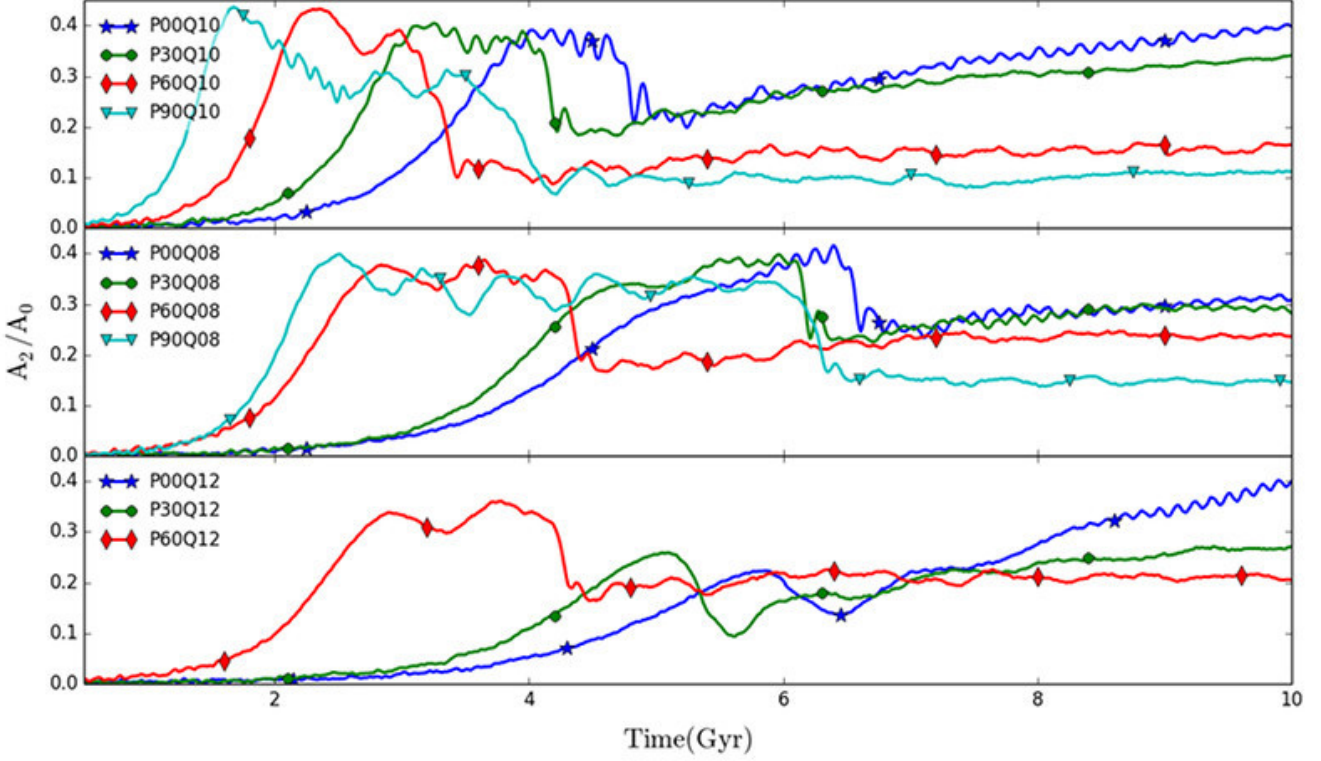


Figure 1. Fourier amplitude A_2 evolution: the λ sequence. Comparing models with the same halo shape for various λ . These amplitudes have been normalized by A_0 . These colours have been explained in the inserts.

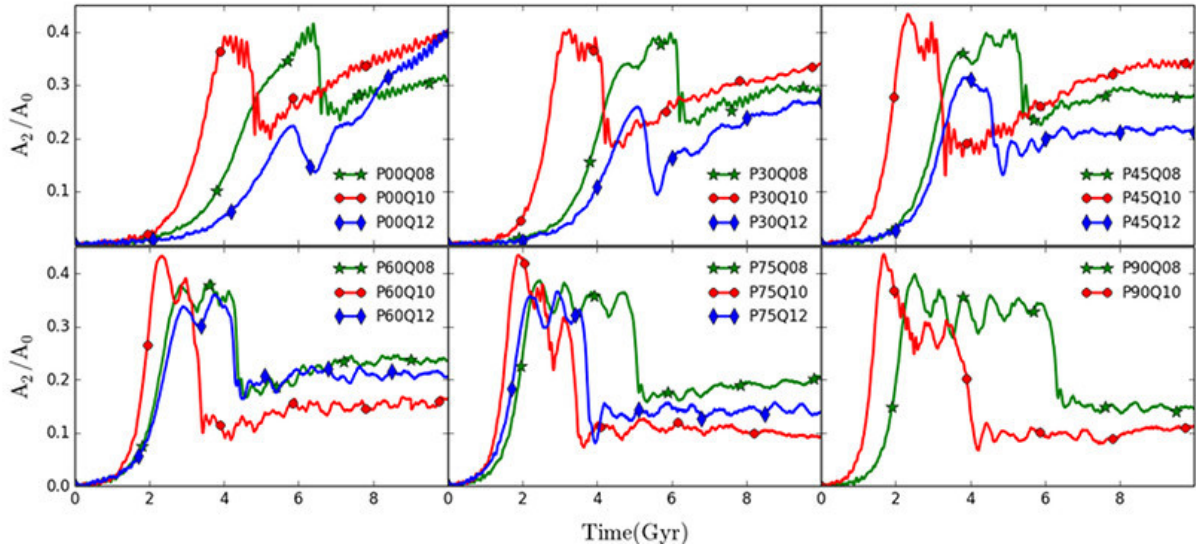


Figure 2. Fourier amplitude A_2 evolution: the halo shape sequence. Comparing models with the same λ for spherical, oblate, and prolate haloes separately. These amplitudes have been normalized by A_0 . These colours have been explained in the inserts.

Another effect observable in Figure 4 is that during the bar instability, *before* the buckling, lower λ models lose angular momentum much faster than in P00 model with a non-rotating halo. The reason for this is that these bars grow faster in the initial stage of the bar instability. Higher λ

models while growing faster, also buckle much earlier and their subsequent growth is suppressed.

Third, Ω_b decreases abruptly during buckling for low- λ models, while stays flat and increases for higher λ models.

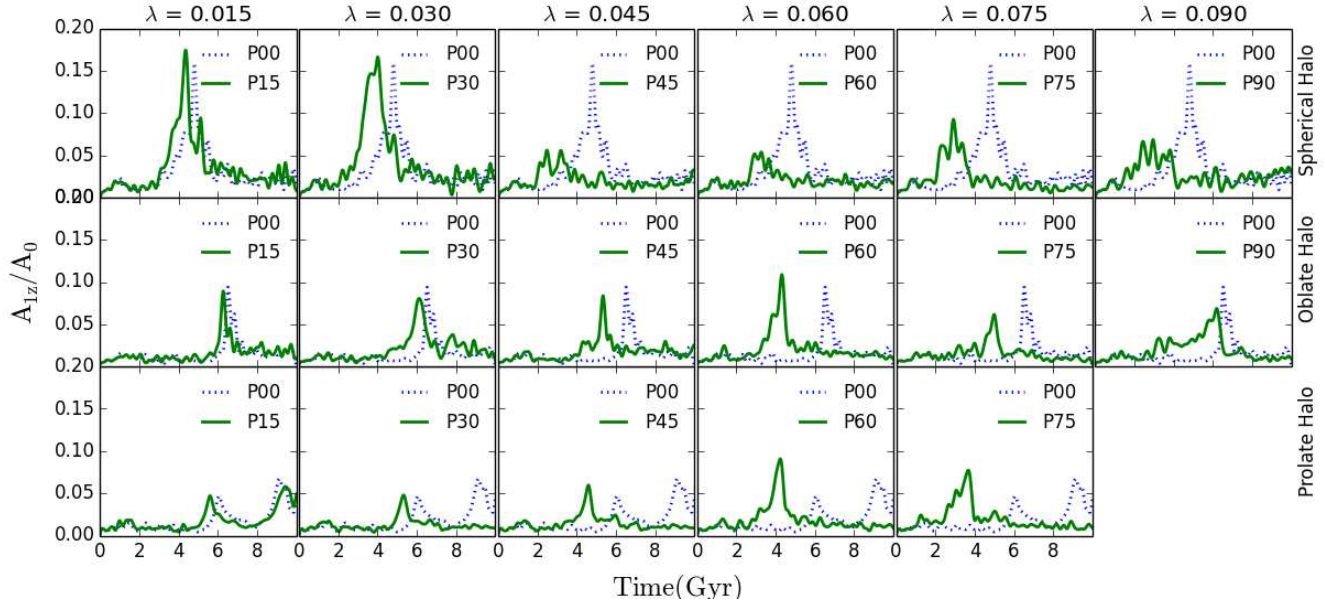


Figure 3. Vertical buckling amplitude of stellar bars, A_{1z} (green line), normalized by A_0 , in spherical (top row), oblate (middle row) and prolate (bottom row) haloes, along the λ -sequence. For a comparison we superpose the buckling amplitude of $\lambda = 0$ models on each λ -sequence (blue line).

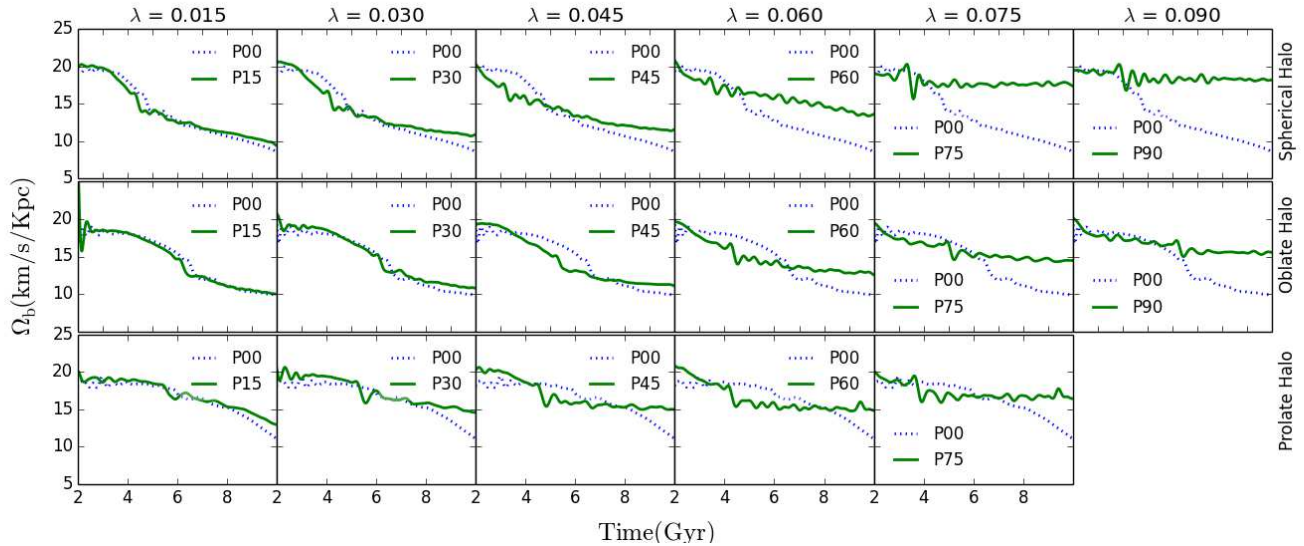


Figure 4. Evolution of bar pattern speeds, Ω_b (green), in spherical (top row), prolate (middle row) and oblate (bottom row) DM haloes and for increasing λ (from left to right), from $\lambda = 0.015$ to 0.09 . For a comparison we superpose the pattern speeds of $\lambda = 0$ models on each λ -sequence (blue).

This appears to be important and we follow up on this point in the Discussion section.

3.4 Bar size evolution in spinning haloes

We have determined the bar size based on the highest Jacobi energy x_1 orbit inside the CR (Martinez-Valpuesta et al. 2006). Such orbits comprise the most important family of orbits supporting the bar density distribution. The x_1 orbits end short of the CR. The character-

istic diagram for the main orbit families has been constructed (e.g., Contopoulos & Papayannopoulos 1980; Heller & Shlosman 1996; Berentzen et al. 1998), see also review by Sellwood & Wilkinson (1993).

Figure 5 (top) shows the evolution of R_b . The longest bars reside in the spherical haloes by $t = 10$ Gyr, but evolution of bars in oblate haloes is very similar. The growth of bars in the prolate haloes is very slow after buckling. Bars in P00 models grow longest and their growth is fastest and monotonic, with an inflection around the time of vertical

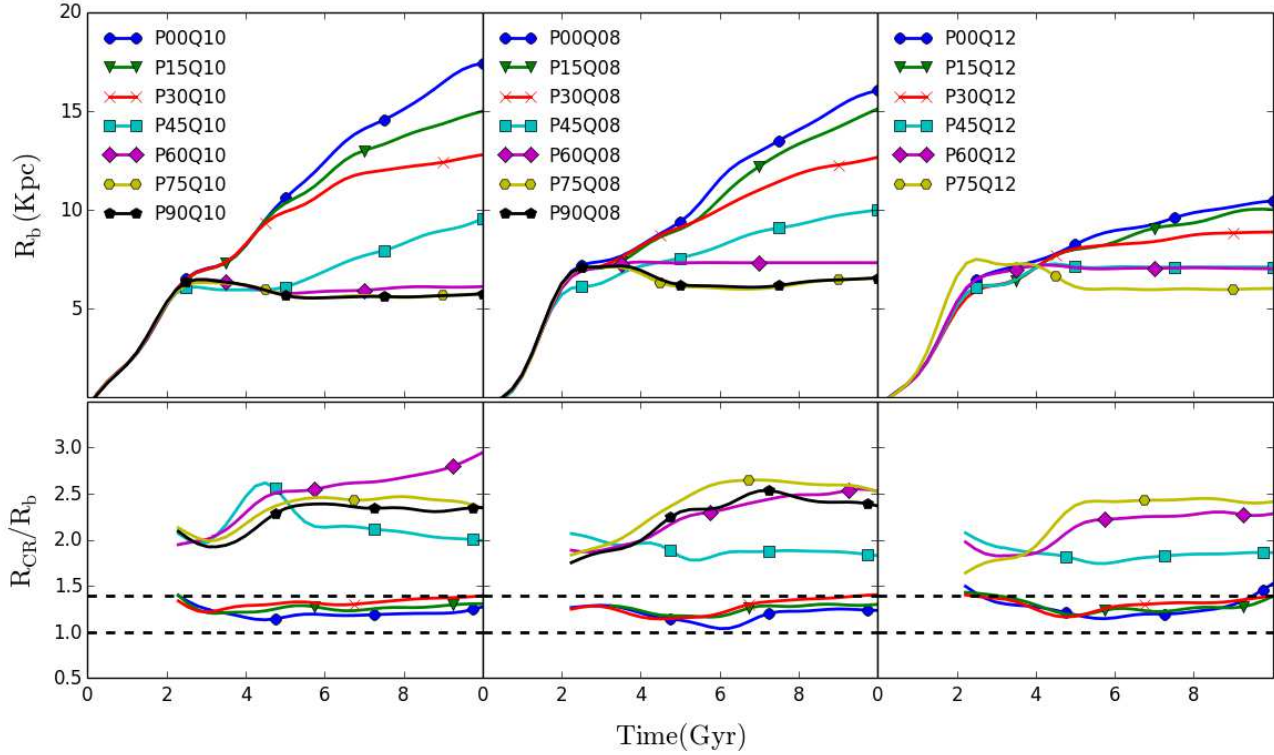


Figure 5. *Top:* Bar length evolution in spherical (left), oblate (middle) and prolate (right) DM haloes. *Bottom:* Bar length-to-CR radius ratio evolution within DM haloes. The dashed lines show the limits for so-called slow bars, $R_{\text{CR}}/R_b = 1.2 \pm 0.2$.

buckling. For $\lambda \gtrsim 0.06$, bars do not grow at all in all models after buckling.

We have also measured the ratio R_{CR}/R_b (Fig. 5, bottom). Bars that extend to the vicinity of the CR, have a narrow range of $R_b/R_{\text{CR}} \sim 1.2 \pm 0.2$, so-called fast bars, while those that fall short of CR are slow bars (e.g., Teuben & Sanders 1985; Athanassoula 1992b). This result has been confirmed in Martinez-Valpuesta et al. (2006), and we reproduce it here for models with $\lambda \lesssim 0.03$ for spherical and oblate haloes. For larger λ , this ratio lies outside the 1.2 ± 0.2 range for the entire time of their evolution. It is also true for prolate haloes with any spin. These bars, therefore, are slow bars, and end well before the CR.

3.5 Angular momentum transfer in oblate, spherical and prolate haloes

Next, we quantify the angular momentum flow in the disc-halo systems which develop stellar bars. In this, we follow the method developed by Villa-Vargas et al. (2009) and Long et al. (2014). This method tracks the total angular momentum rate transfer between the disc and the DM halo, i.e., resonant and non-resonant ones (Athanassoula 2003; Martinez-Valpuesta et al. 2006), but also can reveal the flow between various disc and halo radii. For this purpose, we divide the disc and its host halo into nested cylindrical shells. Then construct a two-dimensional map of the rate of J change in each shell as a function of R and t . The resulting colour-coded maps are shown for spherical, oblate and prolate (Fig. 6) haloes, for the λ -sequence, and the associated stellar discs. The top row in each Figure ex-

hibits the rate of angular momentum flow in DM haloes, $\langle \dot{J}_{\text{DM}} \rangle \equiv (\partial J_{\text{DM}} / \partial t)_{\text{R}}$, while the bottom row, shows the rate of the J flow in the stellar discs, $\langle \dot{J}_{\text{*}} \rangle \equiv (\partial J_{\text{*}} / \partial t)_{\text{R}}$. The brackets indicate the time averaging at R .

The colours in the above Figure represent the absorption/emission (red/blue) of the angular momentum by the DM (top) and disc (bottom) material. The colour palette has been normalised the same way for all discs and (separately) for all haloes. The continuity of these colours represent the emission/absorption of J by the main resonances in the DM haloes and stellar discs, as well as the non-resonant contribution.

The evolution of linear resonances is shown by continuous lines for $\lambda = 0$ models only. For example, the emission of J by the inner Lindblad Resonance (ILR) in the disc follows the lower blue band drifting to larger R with time in model P00Q10 (Fig. 6, lower left frame). The additional blue band corresponds to the Ultra-Harmonic Resonance (UHR). The dominant red band follows the CR and the Outer Lindblad Resonance (OLR).

This Figure is divided into three pairs of horizontal rows representing haloes (top) and discs (bottom), each, for spherical, oblate and prolate haloes. The upper left frame, showing the P00Q10 model, exhibits only absorption (red) by a halo with no or low net angular momentum. However, moving along the λ sequence, we observe profound differences in the absorption/emission of J by both the disc and the halo.

First, we invoke the Standard Model P00Q10 in order to understand the colour palette. The upper frame of Figure 6 displays an intense absorption by the DM halo after

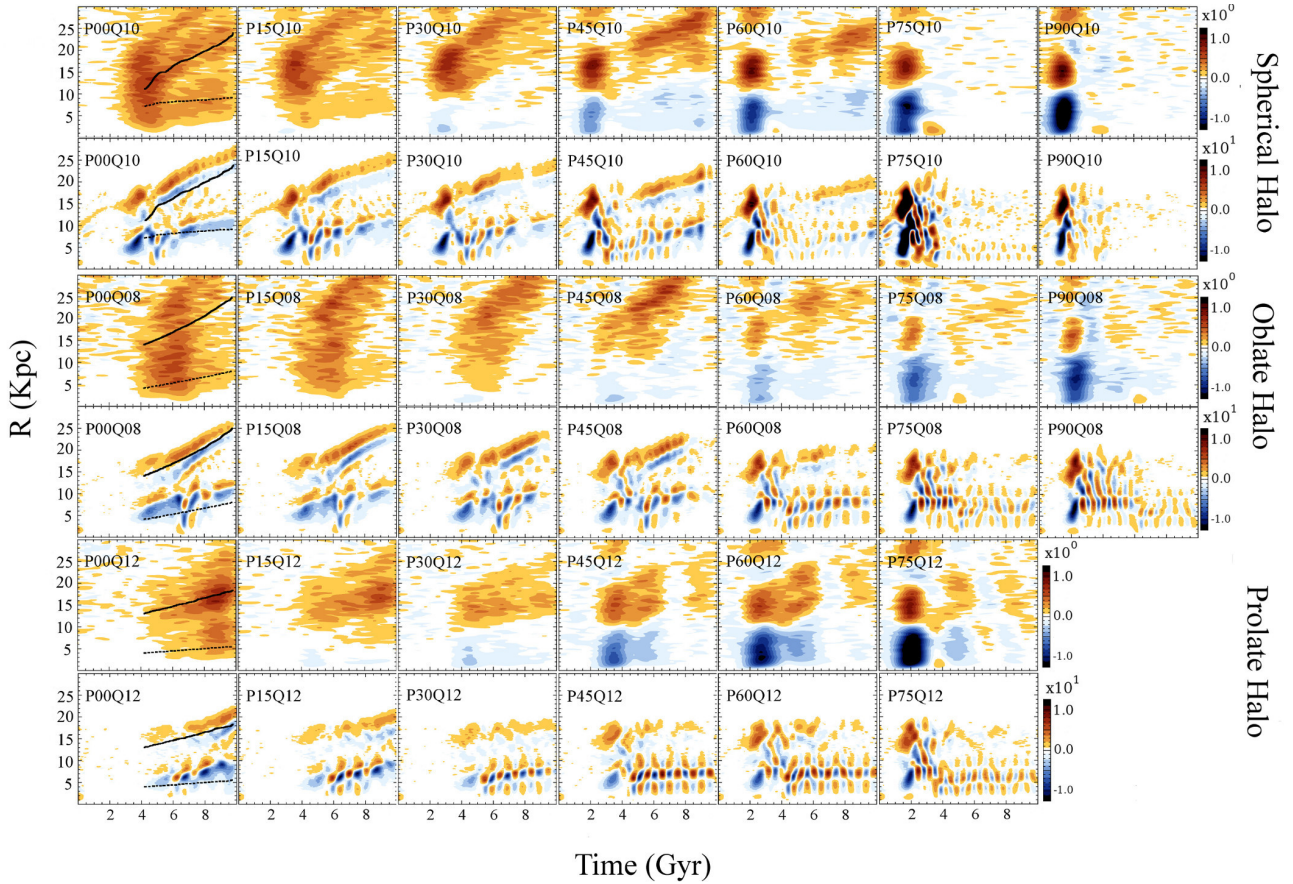


Figure 6. Rates of angular momentum flow, \dot{J} , as a function of a cylindrical radius and time along the λ sequence, for spherical (top two rows), oblate (middle two rows) and prolate (bottom two rows) haloes and the embedded stellar discs. The colour palette corresponds to gain/loss rates (i.e., red/blue) using a logarithmic scale in colour. The cylindrical shells $\Delta R = 1$ kpc extend to $z = \pm 3$ kpc, both for the haloes and their discs. Positions of major linear resonances in the disc, ILR and CR, have been delineated by solid and dashed lines in P00 models.

~ 3 Gyr. This corresponds to the bar strength $A_2 \gtrsim 0.2$ in the Figure 1, for this model. The main region in the halo which participates in this J absorption is within $\lesssim 10$ kpc. So once the bar acquires non-linear amplitude, it facilitates the J transfer to the halo.

For the model P00Q30, this happens earlier, at ~ 2 Gyr. And, what is important, two halo regions participate in the J transfer now: a weak *emission* inside 10 kpc, and absorption between 10–20 kpc. Moving to larger λ , the inner region of the halo emits J , while the outer one absorbs it. The absorption strength stays the same when advancing to P90Q10 while the emission strengthens substantially.

When comparing the maxima of J absorption by the halo with the approximate positions of the main resonances, we observe that the main region between the ILR and OLR dominates the process in the P00Q10. as we move along the λ sequence, the absorption by the ILR disappears and is reversed to emission, while that of the OLR increases. For $\lambda > 0.03$, the ILR starts to emit J . while the absorption is dominated by the CR–OLR region.

In order to demonstrate the efficiency of angular momentum absorption by the DM halo, we have calculated the fractional increase in J for all haloes that have non-zero spin at $t = 0$. Table 1 shows the change in J over the simulation

time, $\Delta J = J(t = 1 - \text{Gyr}) - J(t = 0)$, normalised by $J(t = 0)$. Clearly, along the λ sequences for various halo shapes, this ratio is decreasing. The decrease is significant, e.g., the P90 model haloes acquire about 30 times less angular momentum, compared to P15 models. Hence, the efficiency of J absorption by the haloes along λ sequence decreases.

4 DISCUSSION

We have analyzed evolution of stellar bars in galaxies with spinning DM haloes, with the cosmological spin $\lambda \sim 0-0.09$, which encompasses all the expected range. Various axisymmetric halo shapes have been invoked, namely, oblate, spherical and prolate. We focus on secular evolution of stellar bars under these conditions, and discuss implications for disc evolution.

Our main result is that spinning haloes profoundly affect the bar properties, which was not taken into account so far when addressing galaxy evolution. It was shown recently that the bar instability in axisymmetric disks is accelerated and so is the bar growth during this dynamical phase, i.e., before they reach the maximum strength given by A_2

Table 1. Fractional change in the angular momenta of DM haloes from $t = 0$ to $t = 10$ Gyr for spinning models with increasing λ .

Halo Shape	Halo $\Delta J/J(t = 0)$					
	P15	P30	P45	P60	P75	P90
Spherical	0.1453	0.0633	0.0220	0.0114	0.0047	0.0048
Oblate	0.1373	0.0525	0.0282	0.0115	0.0106	0.0045
Prolate	0.0917	0.0234	0.0099	0.0041	0.0035	

(Saha & Naab 2013; Long et al. 2014). Our main finding is that after bars experience vertical buckling instability, their strength decreases sharply. This decrease is more dramatic for larger λ . Essentially, bars are dissolved for $\lambda > 0.06$, leaving a weak oval distortion behind.

Second, in the subsequent secular phase of evolution, the bar growth, in strength and in size, is severely curtailed with increasing λ . For $\lambda \gtrsim 0.06$, bar growth is completely damped and A_2 remains flat. Next, for $\lambda \lesssim 0.03$, bars extend to near CR, i.e., the ratio of $R_{\text{CR}}/R_{\text{b}} \sim 1.2 \pm 0.2$ remains in the narrow range (i.e., fast so-called bars). For higher λ , this ratio is substantially larger than 1.4, offset dust lanes are not expected and the bars are defined as slow.

Finally, the rate of angular momentum flow from the disc to the DM halo decreases along the λ sequence, after the buckling phase, with J transfer going both ways as shown by the J flow maps. A clear indication of this process is the temporal speed up of the bar tumbling at the end of the buckling instability in higher λ models. This behavior has substantial corollaries to the bar growth — unable to lose its J or even increasing it, the bar amplitude is damped even more, and its pattern speed stops to decrease.

The behaviour of the bar amplitude, A_2 , during the bar instability along the λ sequence has been analysed by Saha & Naab (2013), prior to buckling only, and by Long et al. (2014). The angular momentum transfer from the disc to the halo is amplified due to the increase of the fraction of prograde orbits in the halo which are capable to resonate with the disc orbits. The subsequent secular evolution that has been reported by Long et al. (2014) is confirmed and further analysed in the present work.

What processes accompany the buckling of stellar bars and their subsequent evolution in spinning haloes? We start by focusing on the J redistribution in our models (Fig. 6). The low- λ models, P00 and P15 in all halo shapes, show a pure absorption of J by the DM halos. This absorption is complemented by a strong emission of J by the embedded discs, mostly by their ILRs. Some of this emission is absorbed by the outer disc, but this weakens with time.

However, for higher λ models, emission of J by haloes appears and strengthens with an increasing *inner* halo spin, becoming very strong. At the same time, absorption of J by the haloes shifts gradually to larger R , and the J transfer essentially disappears soon after the buckling. By the end of the buckling, discs exhibit strong absorption in the CR-OLR region, in all models. Hence, we conclude that the J -transfer goes from the disc to the halo in low- λ models, and both ways for haloes with higher spin.

Additional argument in favour of disc receiving J from the halo can be made by analysing Ω_{b} behaviour during

buckling (§3.3). For lower λ , we observe a flattening and a subsequent drop in Ω_{b} , corresponding to the slowdown of the bar, while for larger λ , we see an increase in Ω_{b} , corresponding to a sudden speedup of the bar (Fig. 4). Again, this behavior of Ω_{b} is similar for all halo shapes. In the absence of the gas component, the only source of J under these circumstances is the inner halo.

The angular momentum received by the bar is not only deposited in the tumbling of the bar, but also in the increase of the inner circulation within the bar. Bars that lose J , slow-down *and* become stronger, because loss of circulation leads to increasingly radial stellar orbits within the bar. Similarly, with increase of the internal circulation, the orbits become more circular, and the bar weakens. This additional weakening of the bar, i.e., of its A_2 , contributes to the larger drop in A_2 with increasing λ — the bar receives larger amount of J in haloes with higher spin.

Higher λ haloes in Figure 6 also transfer some of J to larger radii, i.e., ‘talk to themselves.’ Note, that for spinning DM haloes with no discs, such a behavior has been predicted by Papaloizou et al. (1991), based on theoretical analysis. Lower m modes have been stated to be responsible for this evolution. We have followed the development of $m = 2$ modes in the parent DM haloes as well, but unlike the Papaloizou et al. models, this process is controlled by the non-axisymmetric modes in the *disc*. We discuss these modes elsewhere.

As can be seen in Figure 6, the angular momentum transfer between the disc and its halo essentially cease after buckling for larger λ . The oval distortion which remains in the disk does not grow in amplitude A_2 , and so the bar does not reform. We address this issue in the next section.

4.1 Spinup DM halo and bar damping

The central question, is why will the bar not reform after the buckling for a range in λ ? First, we confirm that this is a robust behaviour and not a numerical fluke, and perform additional experiments.

The DM halo has been found to be a recipient of the angular momentum from the barred disc, as discussed in §1. Numerical simulations have determined that this angular momentum transfer from the disc to DM halo involves lower resonances which trap disc and halo particles and amplify their interactions (Athanasoula 2003; Martinez-Valpuesta et al. 2006; Weinberg & Katz 2007a,b; Dubinski et al. 2009). Furthermore, Villa-Vargas et al. (2009) have argued in favour of the dual role played by the DM haloes. Namely, more massive haloes within the disc radius weaken the dynam-

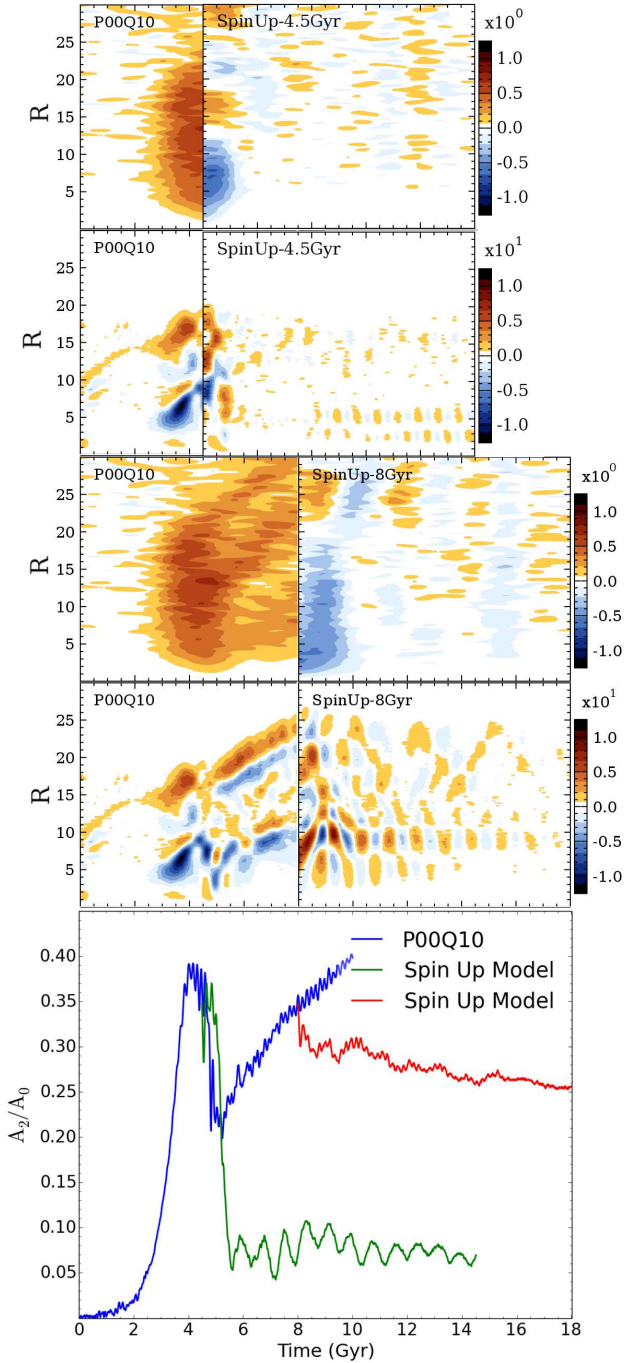


Figure 7. Spinup of DM halo for P00Q10 model to P90Q10 experiments at $t = 4.5$ Gyr and 8 Gyr. (a). Rates of angular momentum flow \dot{J} , as in Figure 6 but before and after the spinup at 4.5 Gyr (top two rows). The left columns correspond to \dot{J} -flow in the P00Q10 model prior to the halo spinup. The right column displays the \dot{J} -flow after the spinup. The top row shows the emission and absorption of \dot{J} by the halo, while the bottom row shows the same for the disc. (b). Same as in (a) but with the spinup at $t = 8$ Gyr. (c). Evolution of A_2 amplitudes, before and after the spinup, and comparison with the P00Q10 model.

ical bar instability, while facilitating the secular growth of the bar. In all these works, the analysis has been limited to non-rotating haloes, mostly of a spherical shape, with rare exceptions (e.g., Berentzen & Shlosman 2006; Athanassoula et al. 2013).

Saha & Naab (2013) and Long et al. (2014) have shown that the bar instability time scale shortens with λ . Finally, Long et al. (2014) have demonstrated that faster spinning haloes damp the amplitude of stellar bars during their secular evolution in spherical haloes. Here we have confirmed these previous works and have shown that the dynamical and secular evolution of bars indeed depend on the cosmological spin parameter of their parent DM haloes.

To confirm that halo angular momentum plays the crucial role in damping stellar bars in spinning haloes, we have performed a number of numerical experiments described below. In the first set of experiments, we have used the spherical non-rotating halo in P00Q10 at $t = 8$ Gyr and 4.5 Gyr, and spun it up to $\lambda \sim 0.09$, i.e., to the halo in P90Q10. This has been performed using the method described in §2.1. In a second set of experiments, shown in the next section, we used the spherical, fast spinning halo in P90Q10, and spun it down to $\lambda = 0$, using the same method (§4.2).

Figure 7 displays the bar amplitude evolution (bottom frame) before and after the halo spinup at $t = 8$ Gyr and at 4.5 Gyr. We have run these models for an additional 10 Gyr, to test their behaviour. Prior to spinup, the stellar bar had been growing secularly, i.e., P00Q10 model, almost reaching its pre-buckling values of A_2 . After the spinup at $t = 8$ Gyr, it stopped strengthening and even started a moderate decay. The middle-top frame displays the rate and direction of the J flow before and after the spinup. Prior to the spinup, the halo had been only absorbing J . After the spinup, it started to emit J , except in the region of $\gtrsim 15$ kpc, which still shows some absorption. If the halo is unable to absorb, the bar cannot grow, and this is exactly what we detect. After $\gtrsim 10$ Gyr, there is basically no exchange of angular momentum in the system.

Prior to the spinup, the disc had been emitting J mainly at its ILR, and switched to absorption after the spinup. For the next 2 Gyr, we observe J flow from the parent halo to the disc. Subsequently, the halo and the disc are not engaged in the J transfer.

Therefore, the spinup of the halo resulted in the angular momentum transfer to the disc for a period of about 2 Gyr, followed by a complete cessation of J -transfer between the two morphological components, *despite existence of a moderate strength bar*.

To further test the bar evolution in spinning haloes, we have repeated the spinup of the DM halo in P00Q10 model at $t \sim 4.5$ Gyr (Fig. 7, top two rows). The main difference with the previous experiment lies in that the spinup happens as the buckling develops. Indeed, the subsequent evolution of the system differs profoundly from the previous experiment — the bar is nearly completely dissolved within ~ 1 Gyr from the spinup. Thus it mimics the evolution of P90Q10 model.

The explanation to this interesting behavior is related to the orbital evolution in the disc during the buckling instability. Martinez-Valpuesta & Shlosman (2004) have shown that the outer part of the bar, beyond the ILR, is dissolved in the buckling, due to the increase of the fraction of chaotic

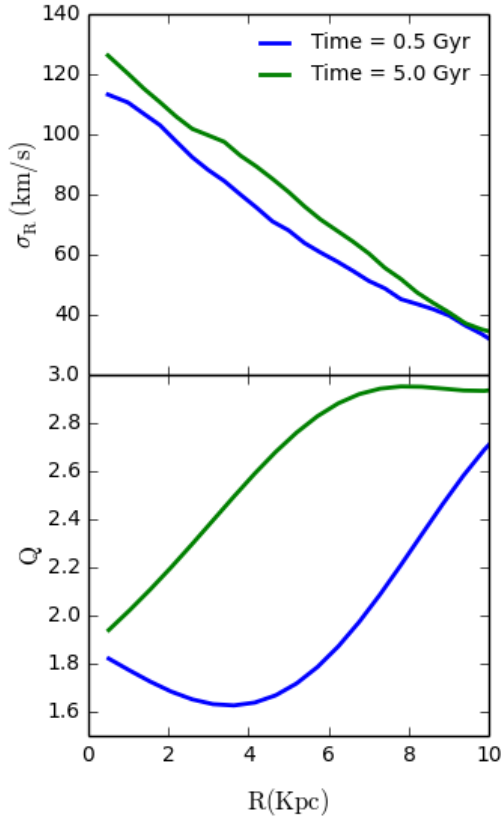


Figure 8. Comparison between σ_R (top) and Toomre’s Q (bottom) for P90Q10 model at $t = 0.5$ Gyr and at $t = 5$ Gyr, following bar vertical buckling and near dissolution. Note that for the former time, the bar did not form yet, and for the latter one, it has dissolved. Hence, this Figure shows either initial σ_R or dispersion velocities of de-correlated orbits in the disc.

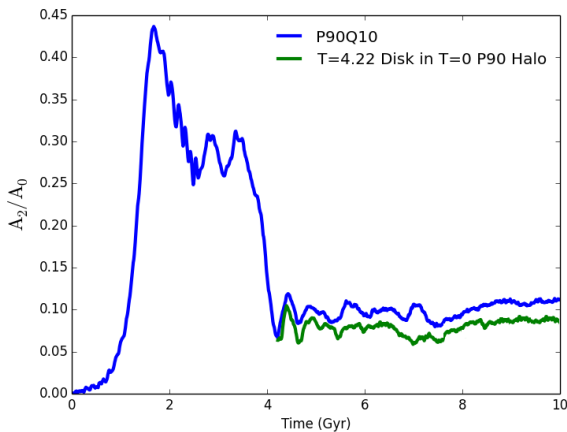


Figure 9. Test: A_2 for P90Q10 model — replacing the DM halo at $t = 4.22$ Gyr. After buckling of the bar the DM halo is replaced by the same halo at $t = 0$. Note that the bar instability is completely suppressed and the $A_2 < 0.1$ and remains flat.

orbits there, as shown by the surface of sections. With an increase of the fraction of chaotic orbits, the area of the regular orbits decreases and the invariant curves which enclose the region of chaotic orbits start to dissolve. Chaotic orbits thus ‘leak’ through the invariant curves at Jacobi energies above the ILR. The bar shortens, but survives and quickly regains its strength by transferring its angular momentum to the parent halo. Thus, the bar survives the buckling, but this statement is limited to nonrotating haloes.

The tandem of buckling instability and spinning haloes leads to a different outcome — the bar amplitude declines more than in the nonrotating haloes, because the combination of the spunup halo and the buckling result in additional decline in A_2 , as discussed above. Dissolution of the bar populates the disc with orbits with large radial dispersion velocities. These orbits have been confined by the bar before the buckling — now they are de-correlated in the absence of the bar.

The relationship between bar dissolution and the fraction of chaotic orbits had been first discussed in the context of the bar strength (Teuben & Sanders 1983, 1985; Athanassoula et al. 1983). For example, bars with axial ratios larger than 5:1 should dissolve as they are dominated by chaotic orbits. Chaotic orbits will diffuse in the phase space being limited only by energy conservation. In other words, they will de-correlate, leading to the bar washing out. So one should expect that such de-correlated orbits from dissolved or even nearly dissolved bars will contribute to larger radial dispersion velocities in the disc.

Returning to the problem at hand, we reiterate the question: what prevents the bar from reforming after buckling in spinning haloes? After all, the disc becomes nearly axisymmetric and the halo is identical to that of P90Q10 halo in the early stage of evolution — conditions under which the bar instability is actually accelerated. If the increase in the fraction of chaotic orbits results in a larger velocity dispersion, then the disc becomes ‘hotter.’

To verify this, we have measured the radial dispersion velocities, σ_R , in the disc at two different times, namely, at $t = 0.5$ Gyr, before the bar instability sets in, and at $t = 5$ Gyr, just after the buckling and the spinup (Fig. 8). The disc at $t = 0.5$ Gyr is ‘colder,’ and its radial dispersion velocities are lower. What is more important is that this can be noticed also by measuring the Toomre’s $Q = \kappa\sigma_R/3.36G\Sigma$ parameter, where κ and Σ are the epicyclic frequency and surface density in the disc, respectively. The condition $Q > 1$ kills the axisymmetric instabilities in the disc, and $Q > 2 - 2.5$ damps the non-axisymmetric instabilities (e.g., Binney & Tremaine 2008). Because, after the stellar bar dissolution, $Q > 2$ everywhere outside the inner kpc, the disk in P90Q10 indeed is too hot to form a bar after buckling.

To further lend support that it is the increased velocity dispersion in the disc that prevents the bar from reforming after buckling, we have performed the following numerical test. We have replaced the spinning halo in P90Q10 model at $t = 5$ Gyr by the spinning halo of P90Q10 model at $t = 0$. As Figure 9 demonstrates, the bar instability is completely suppressed when the disc is immersed in this halo, in a sharp difference with the *same* halo at $t = 0$.

So, the combination of spinning halo and buckling are responsible for damping the bar. This explains why the bar

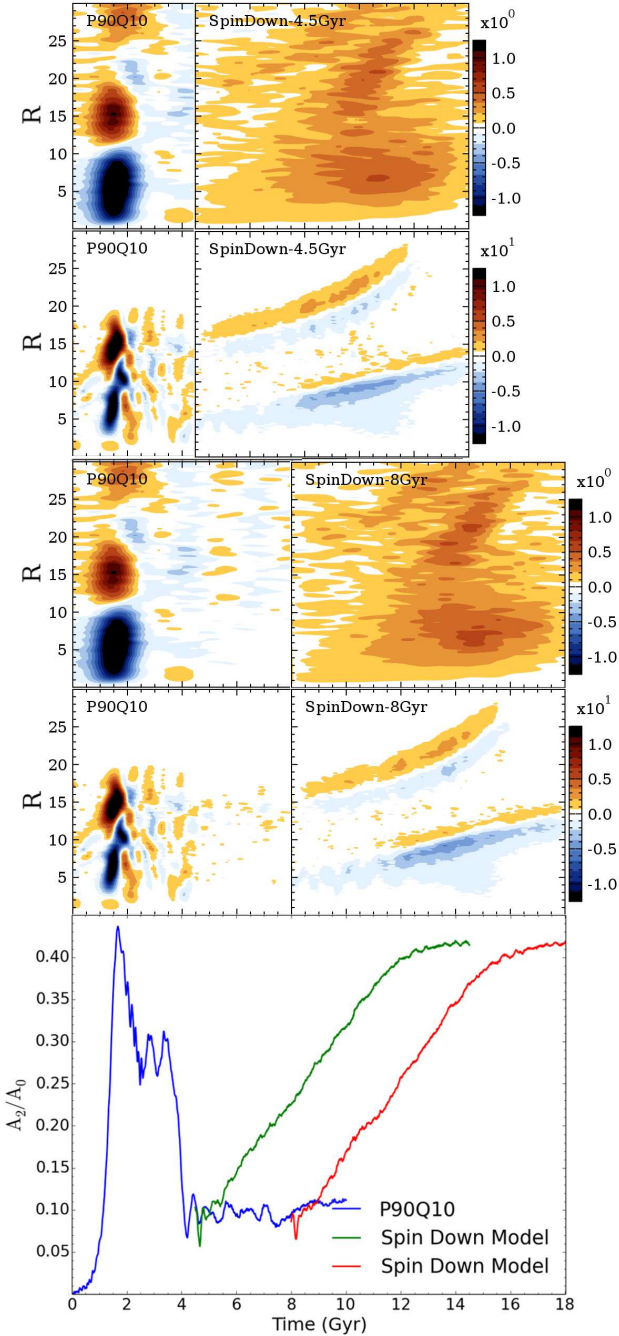


Figure 10. Spindown of DM halo for P90Q10 model to P00Q10 experiment at $t = 4.5$ Gyr and 8 Gyr. Same as Figure 7, but for P90Q10 spindown to P00Q10.

dissolved at 4.5 Gyr, and only slowly decayed at 8 Gyr. The stellar orbits have escaped the dissolved bar at the former time, while remain confined at the latter one.

4.2 Spindown DM halo and bar triggering

The halo spindown tests confirm our reasoning. Figure 10 demonstrates the outcome of the spindown of the DM halo in P90Q10 model to $\lambda = 0$ at two different times, $t = 4.5$ Gyr and 8 Gyr. In both cases the bar instability sets in and a

strong bar develops, exactly as in P00Q10 model, i.e., both test models reach the same peak amplitude, matching the value reached by the standard model, P00Q10.

After the spindown, the halo became active in absorbing the disc angular momentum, as displayed in the maps of angular momentum transfer. At the same time, the disc started to emit its J from the ILR and showed some absorption around the OLR. This behavior clearly demonstrates the effect of the halo spin on the bar strength.

4.3 Observational corollaries of bar evolution in spinning DM haloes

A long list of observational implications follow from our main result — modified stellar bar evolution with increasing DM halo spin. In this work we touch only a few of these corollaries.

In order to estimate the importance of this effect, one should account for the distribution of haloes with λ . Numerical simulations exhibit a lognormal distribution of haloes with λ , with the average of $\bar{\lambda} \sim 0.035 - 0.04$ (e.g., Bullock et al. 2001; Hetzner & Burkert 2006; Knebe & Power 2010).

Bars brake against DM haloes as they tumble, which is accompanied by angular momentum transfer from disc to the DM. As we have discussed earlier, this process involves both resonant and non-resonant J -transfer. During this process, bars grow in size. Thus the bar growth and J -transfer are highly correlated. Figure 11 shows a substantially differing evolution of $R_b - \Omega_b$ correlation along the λ sequence and for various shapes of DM haloes. All models have been run for the same period of time, but occupy different parts of this diagram. Namely, the high λ models cluster at high Ω_b , especially the prolate models.

The most interesting result is the variation of the final pattern speed of the bars with λ . The initial pattern speed in all models is nearly identical. But the final pattern speed has decreased. The value of this decrease varies from a factor of ~ 2 (for $\lambda = 0$ models) to just $\sim 5 - 20\%$ (for $\lambda \sim 0.09$ models) below the initial one. In fact as we have shown earlier, for a timescale of a few Gyr, bars in the intermediate and higher λ range do not brake at all. These bars, therefore, are genuinely fast bars (not in the sense of their size compared to the CR radius, which is addressed below).

Next, it has been determined that the ratio $R_{CR}/R_b = 1.2 \pm 0.2$ is a reliable indicator for the appearance of offset dust lanes in barred galaxies, which represent the standing shocks in the gas flow of fast bars. The lower value comes from the bars being limited by their extent to the CR — orbits beyond the CR are oriented perpendicular to the bar major axis and so cannot support its figure. The upper limit is the result found by Athanassoula (1992a) in 2-D numerical simulations, and represents the slow bars. For larger values of R_{CR}/R_b , the bars are substantially shorter of their CR radius and the dust lanes disappear, as a result of the modified gas flow.

We find that bars residing within DM haloes with $\lambda > 0.035$ exhibit R_{CR}/R_b ratios which lie well outside the parameter space provided above, which accommodates the dust lanes. This is a substantial fraction of haloes, and can accommodate in excess of 50% of barred discs, which, based on the lognormal distribution of λ , should not exhibit offset

Table 2. Average ratios $R_{\text{CR}}/R_{\text{b}}$ for various halo shapes and λ

Halo Shape	Bars regrow $\lambda < 0.035$	Bars do not regrow $\lambda > 0.035$
Spherical	1.26 ± 0.02	2.31 ± 0.15
Oblate	1.24 ± 0.02	2.21 ± 0.15
Prolate	1.28 ± 0.02	2.07 ± 0.15

dust lanes. Table 2 confirms that the cutoff in halo spin represents well the two groups of bars. No dependence on the halo shape has been detected.

The tidal torques theory (TTT) distinguishes between the linear phase, when the haloes acquire their λ and the nonlinear phase. Whether λ grows during the later stage is a matter of an ongoing debate (e.g., Shlosman 2013). The detailed analysis of spin evolution during mergers has shown that for a limited time period λ increases, then, after relaxation of merger products, it decreases to the pre-merger value. This has been demonstrated in Figure 15 of Romano-Diaz et al. (2007), where $\Delta\lambda \sim \pm 0.02 - 0.03$ [see also Hetzner & Burkert (2006)]. The typical time of this relaxation for massive haloes is $\sim 1 - 2$ Gyr.

This timescale should be compared to the time scale of decay/increase of the bar amplitude discussed in §§4.1 and 4.2, which appears to be $\sim 0.5 - 1$ Gyr. Given such a short time scale of bar weakening/strengthening, it is entirely possible that halo mergers can affect the bar evolution, when the stellar disc survives the ordeal.

Formation of *ansae* in barred discs is still an unsolved issue (e.g., Martinez-Valpuesta et al. 2006). We detect *ansae* in our simulations within all halo shapes considered here. They are persistent for discs with stronger bars, whether growing or slowly decaying. For example, *ansae* are present in the slowly decaying bar of Figure 7, after $t = 8$ Gyr. If we ignore the evolution of bars in the pre-buckling phase due to its relatively short time scale, we find *ansae* in spherical haloes up to $\lambda \sim 0.06$, in oblate haloes up to $\lambda \sim 0.045$, and in the prolate haloes up to $\lambda \sim 0.03$.

Finally, the peanut/boxy bulges are the direct outcome of the vertical buckling instability in stellar bars. Moreover, they grow in tandem with the bar growth, as shown by Martinez-Valpuesta et al. (2006). The general trend we observe is that the low λ models exhibit smaller bulges, irrespective of the halo shape. An additional trend, that has been noticed already by Long et al. (2014), is related to the halo shape which changes from boxy/X-shape in low λ models, to boxy in intermediate λ haloes, to peanut shapes in higher λ haloes. One expects that the mass and, therefore, the luminosity of these bulges will decrease along the λ sequence. We defer this analysis to a later publication.

5 CONCLUSIONS

To summarize, we have performed a detailed high-resolution study of stellar bar evolution in spinning DM haloes, in the range of $\lambda \sim 0 - 0.09$. We confirm the accelerated bar instability with increasing λ , as reported previously, and extend these results to oblate and prolate haloes.

Furthermore, we find that secular evolution of stellar

bars in spinning haloes results in damping of their amplitudes along the λ sequence. This leads to a decreased transfer of angular momentum between the disc and its parent halo, and to leveling off the bar pattern speed. Bars within haloes with larger λ have difficulty to re-grow after a buckling instability. For larger λ , the bars essentially dissolve, leaving a weak oval distortion.

While spinning DM haloes have difficulty to absorb additional angular momentum, it is the combination of λ and the vertical buckling instability of stellar bars that has a dramatic effect on the bar amplitude, leading to its additional drop and bar dissolution. The stellar orbits being confined by the bar de-correlate as a result of its dissolution, leaving a ‘hot’ disc behind with large radial dispersion velocities.

Damping bars during their secular evolution leads to shorter (slow) bars with $R_{\text{CR}}/R_{\text{b}} > 1.4$, for $\lambda > 0.03$, in contrast to longer (fast) bars in low spin DM haloes.

Although our simulations do not include the gas component, we expect it to have a minor role in this effect, because the gas is difficult to lock in the resonance due to dissipation. Yet, the gas can act as to weaken the dynamical instabilities, such as the bar instability in the vertical buckling in the bar, as noted by Berentzen et al. (1998).

Broad observational corollaries follow from this effect, of which we have mentioned only a few: $R_{\text{b}} - \Omega_{\text{b}}$ correlation dependence on the λ sequence; absence of the offset dust lanes in a substantial fraction of barred discs, triggering and damping of stellar bars in galaxy mergers not by direct tidal torques but by affecting the halo spin; *ansae* preference for barred discs in low- λ halos; and the shapes of peanut/boxy bulges, their masses and luminosities.

Hence, stellar bar evolution is substantially more complex when cosmological spin is taken into account. The central issue is that this evolution demonstrates that bars can be destroyed by internal processes in disc-halo systems, or with the help of external processes, and challenges the present paradigm that stellar bars are resilient entities.

ACKNOWLEDGEMENTS

We thank Phil Hopkins for providing us with the current version of GIZMO. We are grateful to Sergey Rodionov for help with numerical aspects of initial conditions, and to Alar Toomre and Scott Tremaine for illuminating discussions. We thank our colleagues, Jun-Hwan Choi, Yang Luo, Emilio Romano-Diaz, Jorge Villa-Vargas and Kentaro Nagamine for help with numerical issues. This work has been partially supported by the HST/STScI Theory grant AR-14584, and by JSPS KAKENHI grant #16H02163 (to I.S.). I.S. is grateful for support from International Joint Research Promotion Program at Osaka University. The STScI is operated by the AURA, Inc., under NASA contract NAS5-26555. Simulations have been performed on the University of Kentucky DLX Cluster and using a generous allocation on the XSEDE machines to I.S. We thank Vikram Gazula for help with software installation on the DLX.

REFERENCES

Allgood, B., Flores, R.A., Primack, J.R., Kravtsov, A.V.,

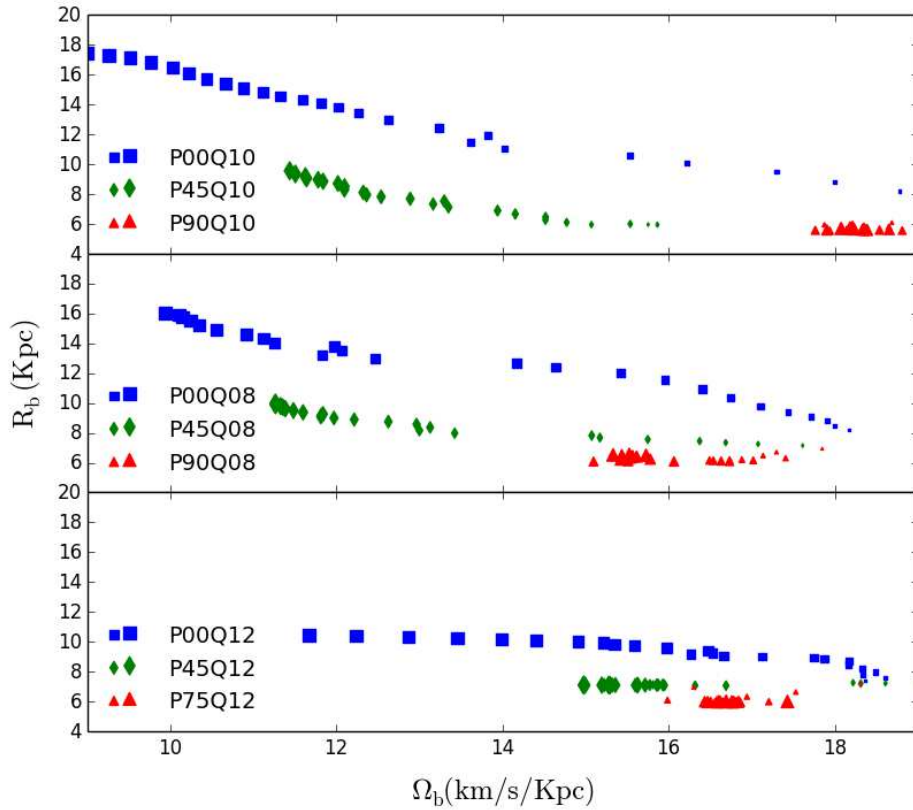


Figure 11. Evolution of the bar length, R_b , versus bar pattern speed, Ω_b for spherical (top), oblate (middle) and prolate (bottom) frames. All models are for $\lambda = 0, 0.045$ and 0.09 . The time direction is given by gradually increasing squares.

Wechsler, Risa, H., Faltenbacher, A., Bullock, J.S. 2001, MNRAS, 367, 1781
 Athanassoula, E., Bienayme, O., Martinet, L., Pfenniger, D. 1983, A&A, 127, 349
 Athanassoula E., Sellwood, J.A. 2006, MNRAS, 221, 213
 Athanassoula, E., 1992a, MNRAS, 259, 358
 Athanassoula, E., 1992b, MNRAS, 259, 345
 Athanassoula, E., 2003, MNRAS, 341, 1179
 Athanassoula, E., 2005, MNRAS, 358, 1477
 Athanassoula, E., Machado, R.E.G., Rodionov, S.A. 2013, MNRAS, 429, 1949
 Berentzen, I., Heller, C.H., & Shlosman, I. 1998, MNRAS, 300, 49
 Berentzen I., Shlosman, I. 2006, ApJ, 648, 807
 Berentzen, I., Shlosman, I., Martinez-Valpuesta, I., & Heller, C. 2007, ApJ, 666, 189
 Binney, J., & Tremaine, S. 2008, Galactic Dynamics, Princeton Univ. Press
 Bullock, J.S., Dekel, A., Kolatt, T.S., Kravtsov, A.V., Klypin, A.A., Porciani, C., Primack, J.R. 2001, ApJ, 555, 240
 Combes, F., Debbash, F., Friedli, D., Pfenniger, D. 1990, A&A, 233, 82
 Contopoulos, G., & Papayannopoulos, Th. 1980, A&A, 92, 33
 Debattista V., Sellwood, J.A. 2000, ApJ, 543, 704
 Dubinski, J., Berentzen, I., Shlosman, I. 2009, ApJ, 697,

293
 Gerin, M., Combes, F., Athanassoula, E. 1990, A&A, 230, 37
 Gilmore, G., Wyse, R.F.G., & Norris, J.E. 2002, ApJL, 574, L39
 Heller, C.H., & Shlosman, I. 1996, ApJ, 471, 143
 Hetzner, H., & Burkert, A. 2006, MNRAS, 370, 1905
 Hohl, F. 1971, ApJ, 168, 343
 Holmberg, E. 1941, ApJ, 94, 385
 Hopkins, P.E., 2015, MNRAS, 450, 53
 Jeans, J.H. 1919, Problems of Cosmogony and Stellar Dynamics, Cambridge
 Knapen J.H., Beckman, J.E., Shlosman, I., Peletier, R.F., Heller, C.H., & de Jong, R.S. 1995a, ApJL, 443, L73
 Knapen J.H., Beckman, J.E., Heller, C.H., Shlosman, I., & de Jong, R.S. 1995b, ApJ, 454, 623
 Knebe C.H., & Power, I. 2010, EAS Publ. Ser., 44, 53
 Kormendy J., & Kennicutt, R.C. 2004, ARA&A, 42, 603
 Larson, R.B. 1984, MNRAS, 206, 197
 Lin D.N.C., Pringle, J.E. 1987, MNRAS, 225, 607
 Long, S., Shlosman, I., Heller, C.H. 2014, ApJL, 783, L18
 Lynden-Bell, D. 1960, MNRAS, 120, 204
 Lynden-Bell D., Kalnajs, A.J. 1972, MNRAS, 157, 1
 Martinez-Valpuesta, I., & Shlosman, I. 2004, ApJ, 613, L105
 Martinez-Valpuesta, I., Shlosman, I. 2005, in The Evolution of Starbursts, AIP Conf. Proc., Vol, 783, p. 189

- Martinez-Valpuesta, I., Shlosman, I., Heller, C. 2006, *ApJ*, 637, 214
- Merrifield, M.R. 2002, in *The Shapes of Galaxies and Their Dark Matter Halos*, ed. P. Natarajan (World Scientific), 170
- Navarro, J.F., Frenk, C.S., & White, S.D.M. 1996, *ApJ*, 462, 563 (NFW)
- Noguchi, M., 1987, *MNRAS*, 228, 635
- Papaloizou, J.C.B., Palmer, P.L., & Allen, A.J. 1991, *MNRAS*, 253, 129
- Patsis, P.A., Skokos, Ch., Athanassoula, E. 2002, *MNRAS*, 337, 578
- Petersen, M.S., Weinberg, M.D., Katz, N. 2016, *MNRAS*, 463, 1952
- Pfenniger, D., Friedli, D. 1991, *A&A*, 252, 75
- Raha, N., Sellwood, J.A., James, R.A., Kahn, F.D. 1991, *Nature*, 352, 411
- Rix, H.-W., Zaritsky, D. 1995, *ApJ*, 447, 82
- Rodionov, S.A., Sotnikova, N.Ya. 2006, *Astron.Rep.*, 50, 983
- Rodionov, S.A., Athanassoula, E., Sotnikova, N.Ya. 2009, *MNRAS*, 392, 904
- Romano-Diaz, E., Hoffman, Y., Heller, C. H., Faltenbacher, A., Jones, D., & Shlosman, I. 2007, *ApJ*, 657, 56
- Saha, K., Naab, T. 2013, *MNRAS*, 434, 1287
- Sellwood, J.A. 1980, *A&A*, 89, 296
- Sellwood, J.A., Wilkinson, A. 1993, *Rep.Prog.Phys.*, 54, 173
- Shlosman, I. 1991, in *IAU Colloq. 124, Paired and Interacting Galaxies*, ed. J. Sulentic & W. Keel (Dordrecht: Kluwer), 689
- Shlosman, I. 2013, in *Secular Evolution of Galaxies*, J.Falcon-Barroso & J.H.Knapen (eds.), Cambridge Univ. Press, 555
- Teuben, P.J., Sanders, R.H. 1983, *Internal Kinematics & Dynamics of Galaxies*, (ed.) E. Athanassoula, Reidel:Dordrecht, p.211
- Teuben, P.J., Sanders, R.H. 1985, *MNRAS*, 212, 257
- Toomre A. 1964, *ApJ*, 139, 1217
- Toomre A., Toomre, J. 1972, *ApJ*, 178, 623
- Tremaine, S., Weinberg, M.D. 1984, *MNRAS*, 209, 729
- Villa-Vargas, J., Shlosman, I., Heller, C.H. 2009, *ApJ*, 707, 218
- Weinberg, M.D. 1985, *MNRAS*, 213, 451
- Weinberg, M.D., Katz, N. 2007a, *MNRAS*, 375, 425
- Weinberg, M.D., Katz, N. 2007b, *MNRAS*, 375, 460